PROCEEDINGS, 48th Workshop on Geothermal Reservoir Engineering
Stanford University, Stanford, California, February 6-8, 2023
SGP-TR-224

Modeling of Distributed Strain Sensing (DSS) in Utah FORGE Stimulations

Ruwantha Ratnayake and Ahmad Ghassemi

University of Oklahoma, Oklahoma

Ahmad.ghassemi@ou.edu; rruwantha13@ou.edu

Keywords: fiber strain, DFN, hydraulic fracturs, FORGE

ABSTRACT

It is planned to install distributed strain sensing (DSS) fiber optics in the production well of Utah FORGE EGS to help assess the rock mass response to stimulation and to characterize its permeability evolution. To date, previous efforts directed towards developing DSS response catalogs have largely focused on simple elastic and planar hydraulic fracturing. However, in fractured rock such as Utah FORGE reservoir, the DSS signature is largely controlled by natural fracture deformation during pumping and production, rather than hydraulic fracture propagation. Therefore, it is important to know the possible strain patterns that the 3D deformation the DFNs would provide. In this study a 3D poroelastic fracture simulator which uses a coupled displacement discontinuity method with a finite element method for fluid flow is used to identify the strain patterns which are caused by different injection rates in the Stage 1 stimulation zone of Utah FORGE. The simulations show a DSS signature which varies in time. The resulting strain signatures are negative at early times and eventually evolve into a positive response as the injection is continued. This is in response to the poroelastic deformation of the fractures. This is further verified by considering the response of a single penny shaped fracture in poroelastic rock, subjected to the same injected rate. It is found that indeed, the tensile zone around the natural fracture edge tip which is responsible for the negative strain, tends to diminish and move away from the fracture center. The opening and unloading of the natural fracture induces a compressive stress in the rock making the zone around the fracture compressive.

1. INTRODUCTION

Hydraulic fracturing technology is widely used in unconventional petroleum reservoirs. The concept has gained popularity in EGS or what we have termed "unconventional geothermal reservoirs" (Ghassemi, 2021). However, the geometry of hydraulic fractures which is crucial for well stimulation are still not adequately understood. Fiber-optic sensing (FOS) is an emerging technology that has gained popularity in the petroleum industry to monitor the geometry of hydraulic fractures. Distributed Strain Sensing (DSS) is such a fiber-optic based dynamic strain sensing technique, which can provide valuable information on stimulated fracture geometry.

A typical DSS system requires a laser interrogator, which generates and sends a laser signal, detects the backscattered light from the formation and converts it to strain measurements at sensing points. (Liu et al, 2020). The distance between these sensing points is called gauge length. These backscattered signals provide information about the axial strain along the fiber cable located in the monitoring well. When compared with other downhole sensors such as geophones, DSS provides information over a wider length and also provides real time measurements.

Strain Calculation

The DSS method measures the linear strain variations along the fiber cable over the gauge length. The strain and the strain rate along a fiber is calculated using the basic strain concept:

$$\varepsilon_{xx}^{i} = \frac{u_x^i - u_x^{i+1}}{L}$$

and the strain rate is given by its time derivative:

$$\dot{\varepsilon_x} = \frac{d\varepsilon_x}{dt} = \frac{\varepsilon_x^{n+1} - \varepsilon_x^n}{t^{n+1} - t^n}$$

Where x indicates the direction along the fiber cable, i indicates the location of sensing point, n indicates the time step index, u_x is displacement in the direction along the fiber, and L is the gauge length.

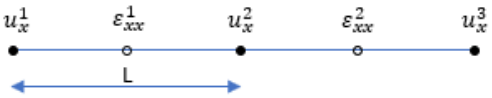

In petroleum engineering applications, strain patters of single and multiple hydraulic fractures are of interest so that much effort has been devoted to developing a catalogue of signatures corresponding to a single and multiple propagating hydraulic fractures (e.g., Ugueto et al. 2021; Liu et al. 2020; Tan et al. 2021; Zhang et al. 2020) using simple elastic analysis of planar fracture. The approach is illustrated in the first example below.

Consider a planar hydraulic fracture propagation towards a monitoring well in which fiber has been installed (Figure 1). The fracture used was 20m in length and 10m in height. Each fracture was discretized with 200 elements (1m×1m). The injection rate used was 5 liters/sec for case 1 and 10 liters/sec for case 2. In case 2 the spacing between the fractures was 10m. A time step value of 300 seconds was used for better accuracy.

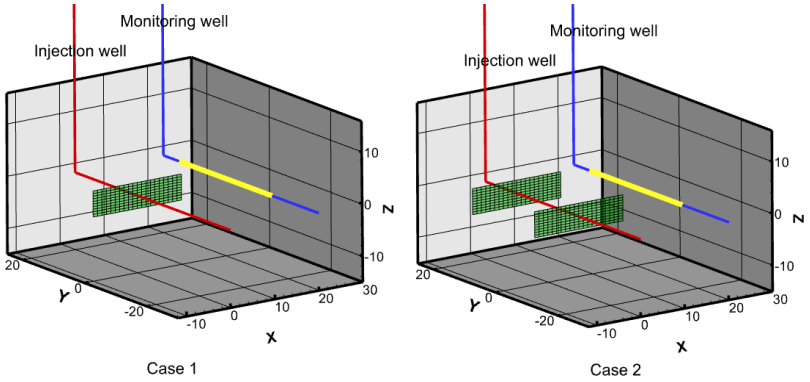

Figure 1: Initial positions of wells and fiber (yellow) with respect to hydraulic fractures in case 1 and case 2.

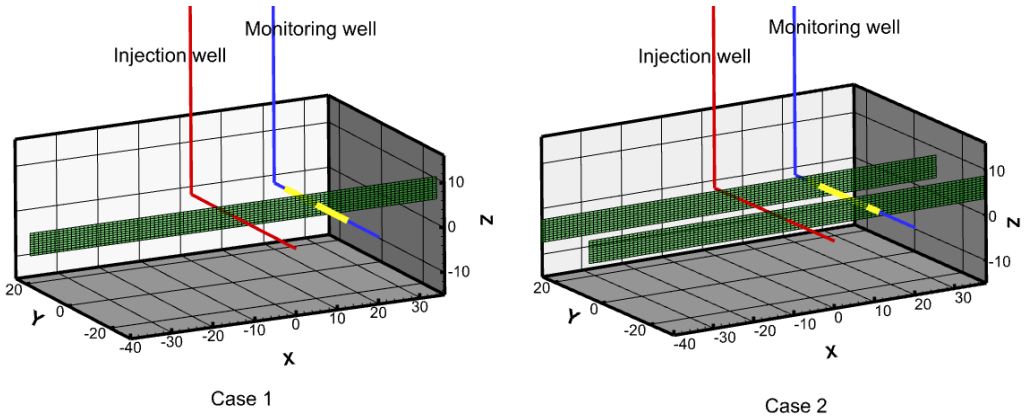

Figure 2: Final configuration of hydraulic fractures (after propagation) in case 1 and case 2.

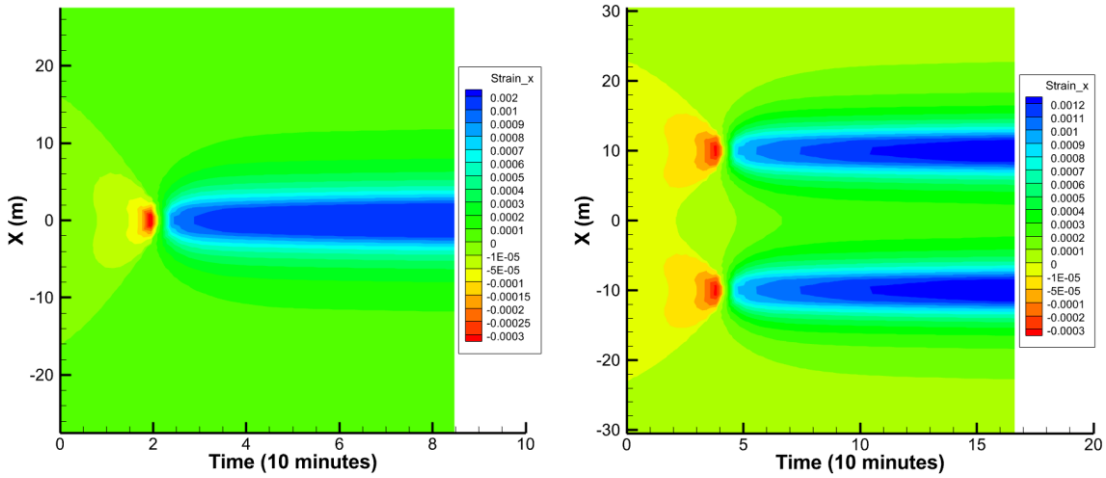

(a) **(b)**

Figure 3: Strain signature for a (a) single fracture, (b) multiple fractures.

Figure 2 shows the final orientation of the fractures in both cases after the propagation. The final dimensions of each fracture were 70m in length and 10 m in height. The fractures were propagated only in horizontal direction. Figure 3(a) shows the obtained strain field for case 1 which is the base case. The plot clearly indicates two parts, around the fracture tip and around the hydraulic fracture. A heart shaped tensile zone exists in the vicinity of the fracture tip and a compressive zone is seen around the fracture walls due to the pressurization. Figure 3(b) shows the strain signature of two parallel fractures with a spacing of 10m hitting the fiber at the same time. As can be seen from Figure 3(b) the same heart shaped region observed in case 1 and the compressional zone exists in both fractures. As indicated before, these signatures cannot be used to distinguish the strain patterns caused by multiple natural fractures oriented in various directions as can occur in Utah FORGE. Also, one would expect the signatures of natural fractures/joints to be different from hydraulic fractures. Therefore, it is interesting to see what signatures a DFN will provide in FORGE and how they are different with signatures given by hydraulic fractures.

2. UTAH FORGE STIMULATION

In this section we calculated the potential magnitude of the strain at the toe of the production well as a function of injection rate into the injection well. The injection well 16A of FORGE has had three stages of simulation and in this study, we focus on Stage 1 which is an open hole section of 196 ft total length. The DFN used in the study was obtained from the Utah FORGE Team and is subject to revision based on the MEQ data. The objective is to help characterize the flow geometry (fracture network) using a planned controlled pumping experiment.

It is expected that the pumping experiments will not result in significant fracture propagation, rather the pumping pressure will remain below the $S_{h,min}$ and thus will only dilate the natural fracture with possible shear deformation. This process can be impacted by pore pressure diffusion and poroelastic effects, so that we use a poroelastic displacement discontinuity method to calculate the strain in the production well in Utah FORGE field. It should be emphasized that to date no such approach to strain measurement and calculation has been attempted. Figure 4 shows the position of the injection and production wells. The natural fractures that intersect the production well and form a network are also shown (using the DFN constructed in the Utah FORGE conceptual model of the reservoir). The production well is assumed to be 300ft above the injection well based on current drilling plans. A fiber cable is planned to be placed in the production well as shown in Figure 4 and is used to record the strain caused by injection into the Stage 1. The cable used for the simulation is assumed to be 55m in length and the distance between two sensing points (i.e., the gauge length) is assumed to be 1m. Therefore, a total of 56 sensing points is assumed to exist along the cable. Table 1 shows the input properties used. Two scenarios are considered using constant injection rates of 10 liters/sec and 1 liter/sec. The injection is carried out for a total of 5 hours with a time step of 15 minutes which means strain was recorded at each 15 minutes of time. In this study compression is considered positive and tension negative.

Table 1: Input data for the study (Ratnayake & Ghassemi, 2022)

G	Shear Modulus	2.088×10^4	MPa
v	Poisson's ratio	0.29	-
v_u	Undrained Poisson's ratio	0.35	-
B	Skempton's pp coefficient	0.47	-
α	Biot's effective stress coefficient	0.69	-
k	Permeability	4.5×10^{-5}	Darcy
c^f	Fluid diffusivity	3.08×10^{-5}	m^2/s
φ	Porosity	0.05	-
μ	Fluid viscosity	1.00×10^{-3}	Pa.s
S_h	Minimum horizontal stress	43.11	MPa
S_H	Maximum horizontal stress	59.77	MPa
S_v	Vertical stress	64.96	MPa
-	Duration of injection	5	hours

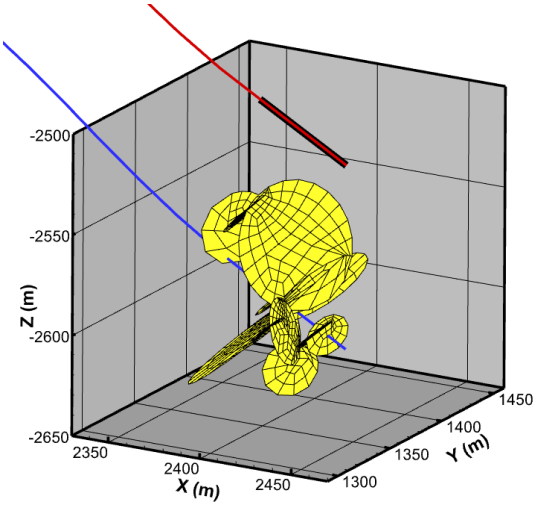

Figure 4: Position of Injection (blue) and production (red) wells with zone 1 fractures and fiber cable (highlighted in black).

3. RESULTS AND DISCUSSION

Figure 5 (a) shows the calculated strain expected to be recorded in the fiber with time as a result of fluid injection at a rate of 10 liters/second into stimulation zone 1. X is the distance measured along the fiber in the axis parallel to the production well where x=0 is the toe of the production well. As can be seen from the plot the recorded strain ranges from $-1x10^{-6}$ to $1.5x10^{-5}$. At early times the recorded strain is closer to $-1x10^{-6}$ at the toe of the well, and as time increases it goes up to $1.5x10^{-5}$ at the topmost end of the fiber. This reflects the natural fracture opening deformation and the corresponding induced stresses in the surrounding rock due to the increase of apertures in fractures in zone 1. Figure 5 (b) shows the calculated strain at the fiber when the fractures are injected with a rate of 1 liter/second. As can be seen the values of the strain recorded are one order of magnitude less than the 10 liters/second case which means a considerable strain response can be recorded even if the fractures are injected at a rate of 1 liter/second.

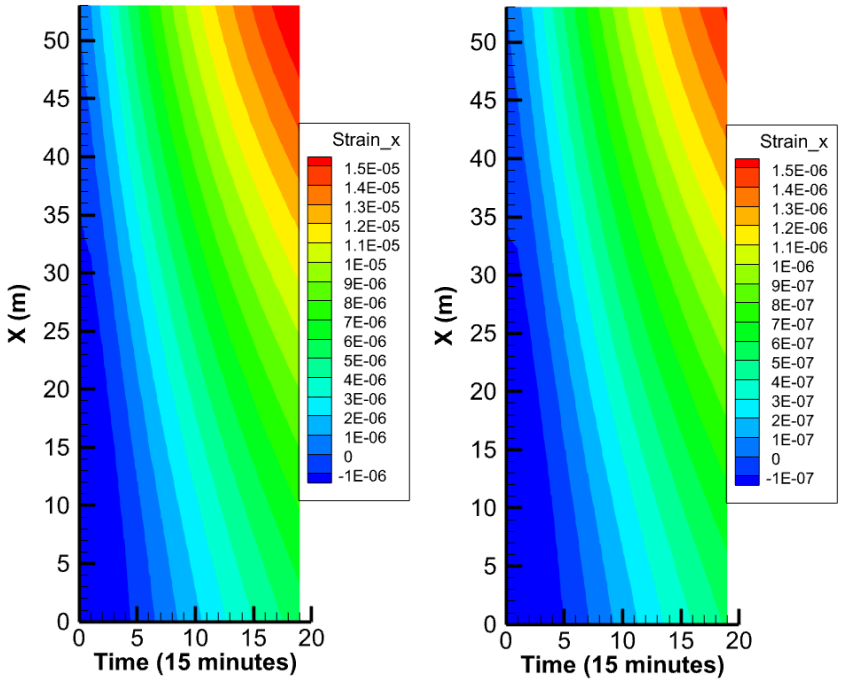

(a) **(b)**

Figure 5: Recorded strain with time for (a) 10 liters/sec (b) 1 liter/sec.

Figures 6-7 show the variation of fracture aperture in the DFN with time for both injection rates. These results can be used to get an idea about the extent each fracture has contributed to the strain response. The fractures with a high fracture opening contribute more by inducing a higher stress in the surrounding rock. When comparing the results, the higher injection rate has opened more fractures and the fracture aperture is higher compared with the lower injection rate. In both cases the apertures of fractures that are located above the injection well are higher than that of fractures below the well. This is because the fracture network portion below the well intersects with the wellbore at just one location while the upper part of the fracture network intersects at multiple points. Therefore, it takes more fluid and has a higher contribution to the recorded strain.

It is interesting to observe in Figure 5 that in both cases the strain is negative at early times, and it becomes positive as the injection continues. A negative strain occurs from tensile stresses that occur at the fracture tip when fractures open. For a propagating hydraulic fracture, one would expect a continuous negative strain in the fiber until it is intersected by the hydraulic fracture. However, this is not the case here even though as can be seen in Figures 6 and 7, fractures apertures continue to increase with time. This can be contributed to the fact that in this case, the natural fractures are gradually pressurized, causing them to dilate while still remaining mechanically closed under the action of the in-situ stress. To illustrate this, consider a single circular natural fracture with 50m radius subjected to injection at a rate of 1 liter/sec. Two cross sections in the rock (horizontal and vertical) are also considered for close examination of the stress field in the vicinity of the fracture. Figure 8 illustrates the fracture, wellbore, fiber (red) and the cross sections around the fracture. A time step of 5 minutes was used to get a more accurate measurements and the injection was carried out for 5 hours. The cross sections, recorded strain in the fiber and the fracture aperture variation are plotted and shown in Figures 9,10,11 and 12, respectively.

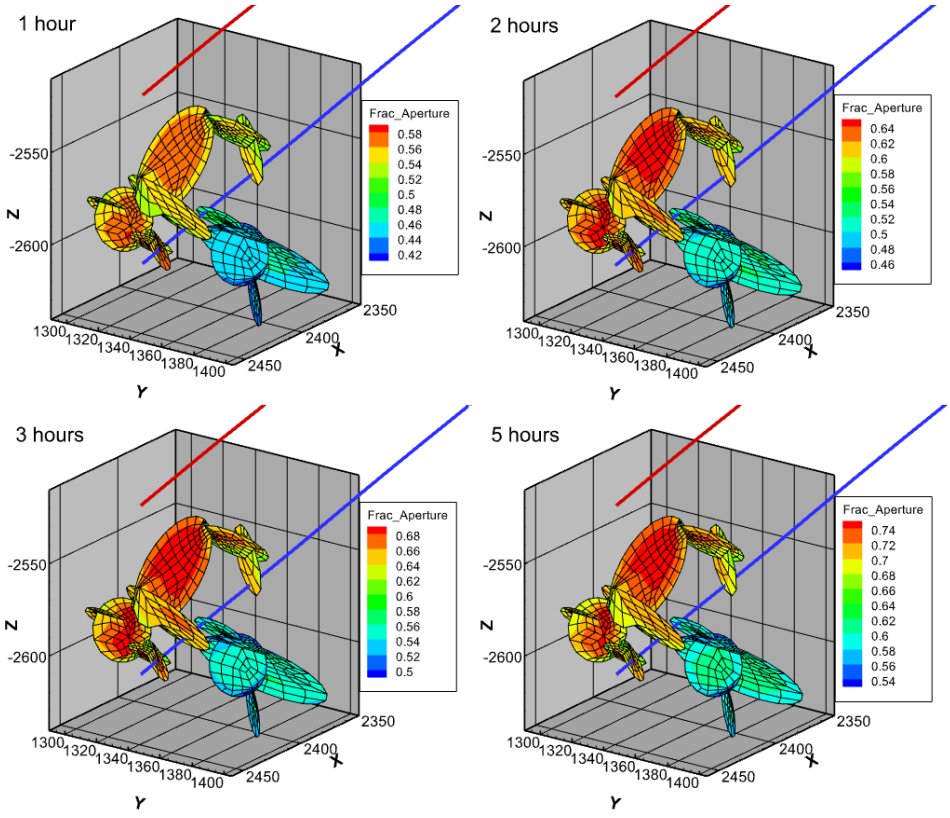

Figure 6: Variation of fracture aperture with time for 10 liters/sec.

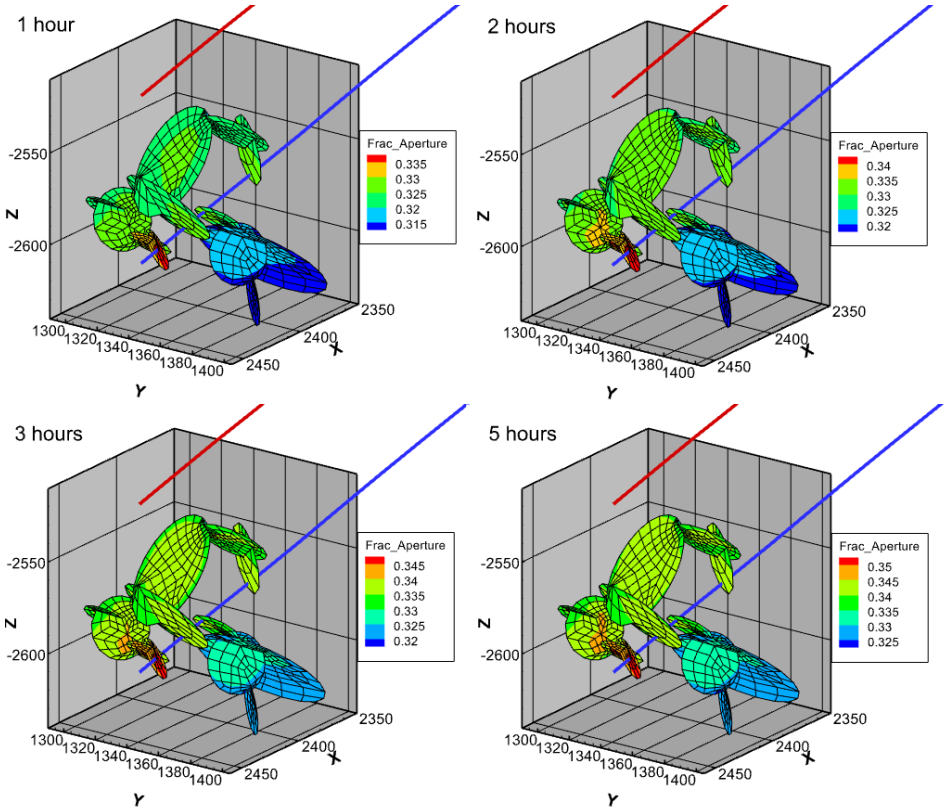

Figure 7: Variation of fracture aperture with time for 1 liter/sec.

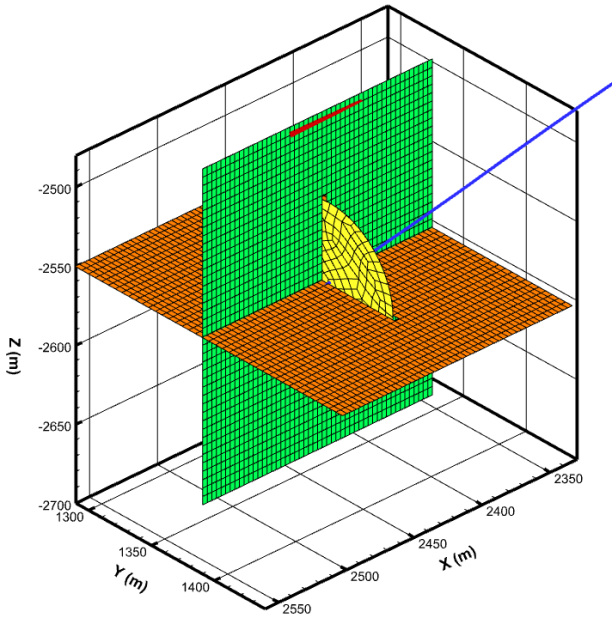

Figure 8: Position of penny shaped fracture, injection well, fiber (red) and the cross sections.

As can be seen since the injection rate is small when compared to the fracture size, a small portion of the fracture near the injection point dilates first and a tensile zone develops on the edge of the opened section while the rest of the fracture remains closed. The injection rate is intentionally kept low to avoid fracture propagation. As the injection continues, the natural fracture aperture

increases (refer Figure 12) and develops a zone of compression in the vicinity of fracture wall due to the stress shadow associated with the NF dilation. It can also be observed from Figure 9 that as the area of compression increases, the magnitude of tension at the tip shows a movement away from the fracture. By 5 hours of injection the tensile zone has moved further away from the fracture and most of the area around the fracture is in compression. This can also be verified with the strain recorded in the fiber shown in Figure 10 where the tensile strain increases to a maximum somewhere around 80 minutes and then starts decreasing. The main reason for this movement is fracture dilation. As pressure increases, the fracture aperture increases and induces a compression zone in the surrounding rock walls. As dilation increases, the size of the compression zone increases and because of its high magnitude (10 times higher than tensile strain) it pushes the tensile zone away from the fracture dilated zone. These results clearly explain the reason why the strain response of the DFN was negative (tensile) at early times and positive (compressive) as injection continues. Figure 11 shows the induced stresses on the horizontal cross section and as expected the pattern is similar to that recorded on the vertical cross section.

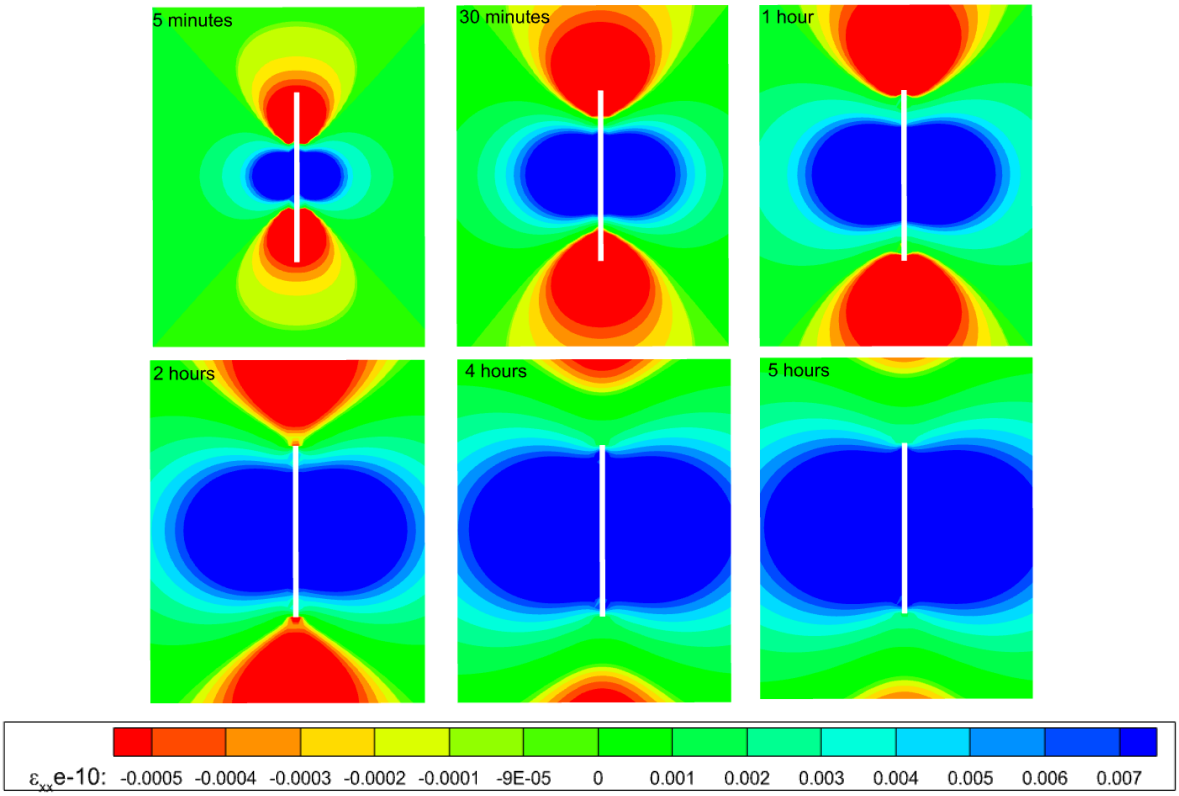

Figure 9: Recorded induced strain in the vertical cross section at different times.

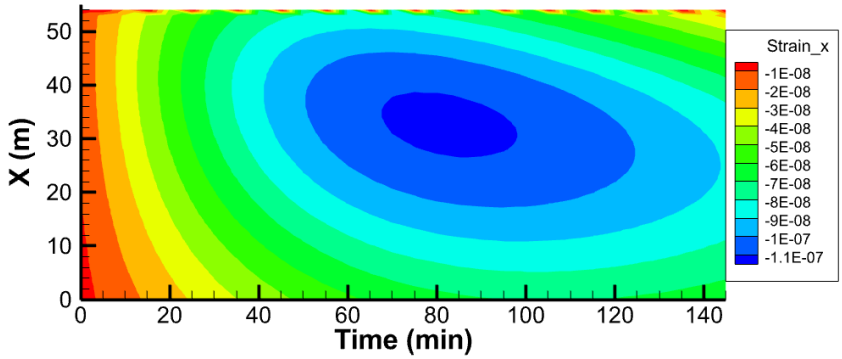

Figure 10: Recorded strrain in the fiber at different times.

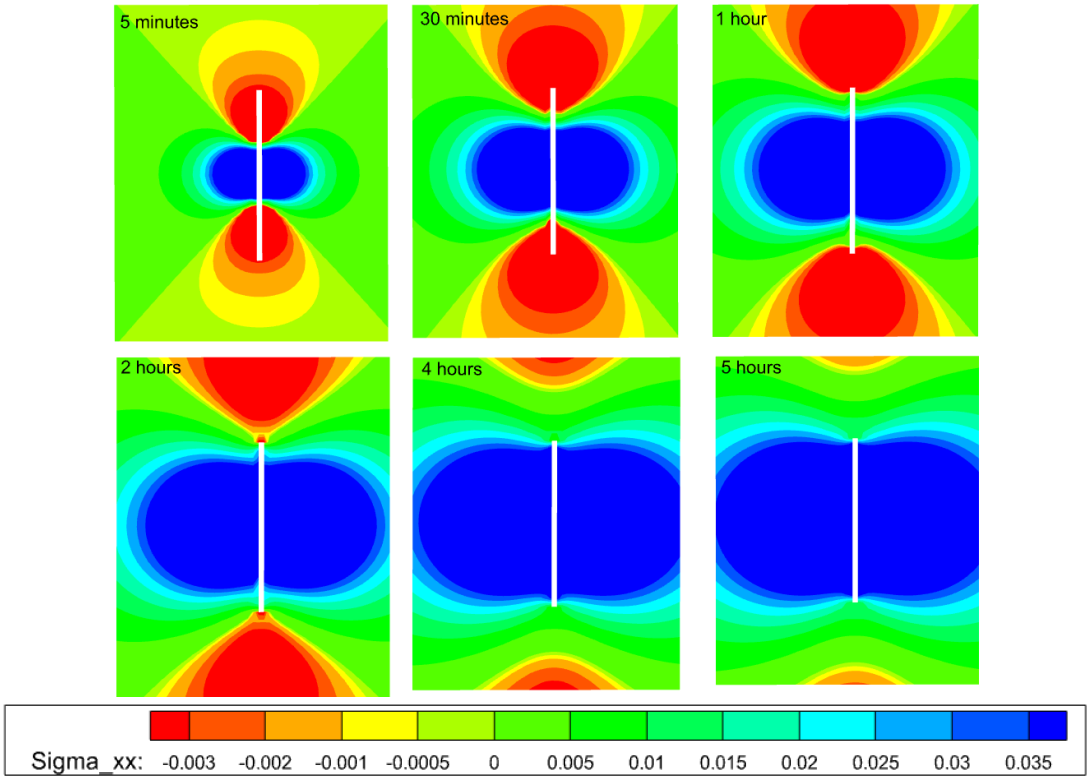

Figure 11: Induced stresses in the horizontal cross section at different times.

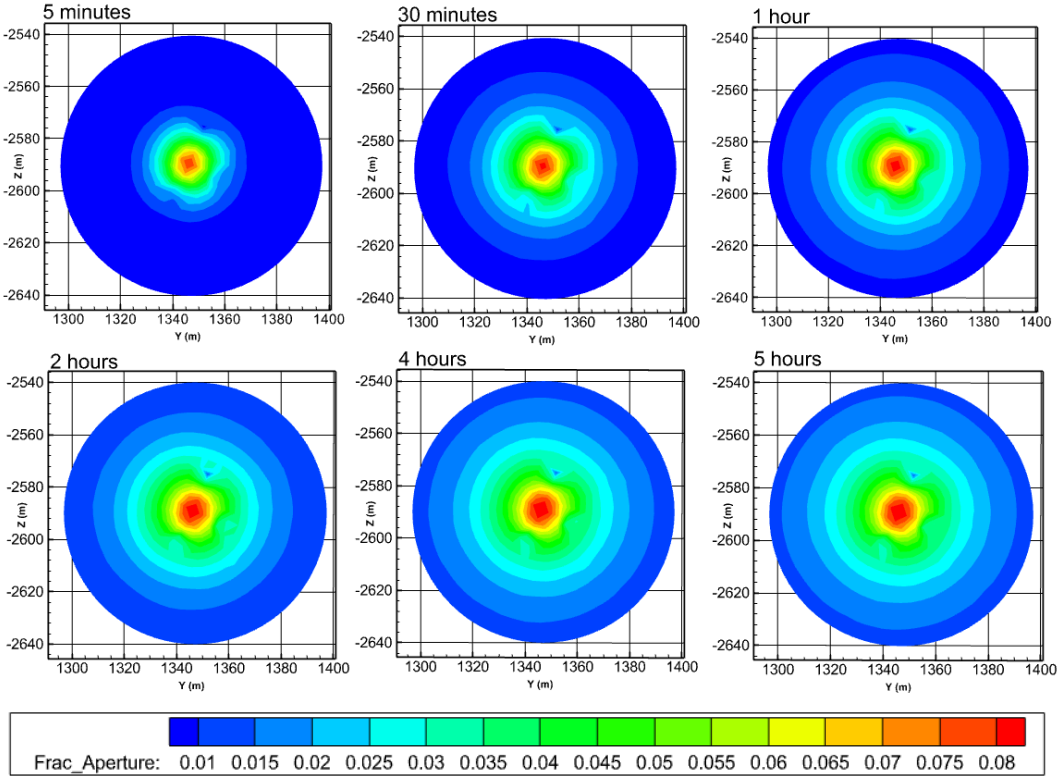

Figure 12: Variation of fracture aperture (mm) with time for the single fracture.

4. CONCLUSION

In this study we examined the fiber strain response near stimulated natural fractures using a 3D poroelastic DD method with application to Utah FORGE Stage 1 stimulation. To estimate the expected strain magnitude and its pattern 300 ft above the injection well, two different injection rates were used in the simulations. Both injection rates (10 liters/sec and 1 liter/sec) gave noticeable strain signature in the fiber. The results show an interesting strain pattern with an initial tensile strain (negative) evolving into a positive response (compression) as the injection continued. This phenomenon reflects the fact that dilation process of natural fractures is quite different from those of propagating hydraulic fractures.

REFERENCES

Ghassemi, A. (2021). Enhanced Geothermal System: The Unconventional Geothermal Resource. Special Presentation. *URTeC.*

Ugueto, G. A., Magdalena, W., Sommnth, M., Artur, G., Dana, J., & Ge, J. (2021). New Fracture Diagnostic Tool for Unconventionals: High-Resolution Distributed Strain Sensing via Rayleigh Frequency Shift during Production in Hydraulic Fracture Test 2. *URTeC.* Houston.

Liu, Y., Wu, K., Jin, G., Moridis, G., Kerr, E., Scofield, R., & Johnson, A. (2021). Fracture-Hit Detection Using LF-DAS Signals Measured during Multifractur Propagation in Unconventional Reservoirs. *SPE*, 523-535.

Ratnayake, R., & Ghassemi, A. (2022). The Role of Thermo-Poroelastic Effects in Utah FORGE Stimulation Experiments. *GRC.* Reno.

Tan, Y., Margaretha, S., Rijken, M., Hughes, K., Ning, I., Zhang, Z., & Fang, Z. (2021). Geomechanical Template for Distributed Acoustic Sensing Strain Patterns during Hydraulic Fracturing. *SPE Journal.*

Zhang, Z., Fang, Z., Stefani, J., DiSiena, J., Bevc, D., Ning, I., . . . Tan, Y. (2020). Fiber Optic Strain Monitoring of Hydraulic Stimulation: Geomechanical Modeling and Sensitivity Analysis. *URTeC.* Austin.